Wavelength tunability of second-harmonic generation from two-dimensional $\chi^{(2)}$ nonlinear photonic crystals with a tetragonal lattice structure

L.-H. Peng[a] and C.-C. Hsu
Department of Electrical Engineering and Institute of Electro-Optical Engineering, National Taiwan University, Taipei, Taiwan, Republic of China

Jimmy Ng and A. H. Kung
Institute of Atomic and Molecular Sciences, Academia Sinica, Taipei, Taiwan, Republic of China

(Received 17 November 2003; accepted 26 February 2004)

The wavelength tunability of second-harmonic generation (SHG) in a two-dimensional nonlinear photonic crystal (2D NPC) on lithium niobate is examined by using a 1.55 μm-band optical parametric oscillator. We observed SHG signals that were generated off-axis from the fundamental pump beam and a multiple number of quasi-phase-matchable (QPM) wavelengths for a given crystal setting. The spacing between the phase-matched wavelengths increases with the azimuthal rotation angle (ϕ) in the $x-y$ plane of the crystal. The peak intensity and propagation direction of the SHG signals are found to vary with the pump wavelength and crystal rotation angle. These observations are ascribed to a 2D distribution of high-order reciprocal lattice vectors $\mathbf{G}_{mn}(\phi)$ and the corresponding $\chi^{(2)}(\mathbf{G}_{mn})$ nonlinearities in 2D NPC having a tetragonal structural symmetry. © *2004 American Institute of Physics.* [DOI: 10.1063/1.1728303]

The use of the quasi-phase-matching (QPM) technique to enhance nonlinear wave interactions has been actively pursued in nonlinear optics. A QPM structure can be realized in ferroelectric nonlinear crystals by seeking a periodic domain reversal at every coherent length $l_c=\lambda_\omega/4(n_{2\omega}-n_\omega)$.[1] Such material modification can lead to a periodic sign change in the $\chi^{(2)}$ nonlinearity and render a structure-imposed phase factor to compensate the destructive interference caused by the crystal's optical dispersion as the interacting waves propagate in the crystal. This compensation can result in a constructive nonlinear process and provide an efficient means for laser wavelength conversion.[2] Recent realization of QPM optical parametric oscillators (OPO) and second-harmonic generators (SHG) using periodically poled lithium niobate (PPLN)[3] and potassium titanyl phosphate (PPKTP),[4] are representative developments in this field. A stringent limitation of these one-dimensional (1D) periodically poled QPM devices, however, is their wavelength agility. Let's take the QPM-SHG process as an example. For a given temperature and incident angle, efficient SHG can only occur at a single wavelength that fulfills the momentum conservation condition, $2\mathbf{k}_{1\omega}+\mathbf{G}=\mathbf{k}_{2\omega}$, where the $\mathbf{k}_{i\omega}$'s are the wave vectors at the fundamental- and second-harmonic frequencies, respectively, and $\mathbf{G}=\pi/\Lambda$ is the reciprocal lattice vector resulting from a first-order QPM structure with a periodicity of 2Λ. In addition, the temperature and wavelength acceptance bandwidths are very tight. The tolerance is approximately equal to Λ/l ($\sim$0.1%), where l is the length of the crystal.[5] These effects add to the complexity in using such devices to achieve simultaneous multiwavelength switching/conversion that often is needed in applications such as optical information processing[6] and telecommunication.[7]

An approach to overcome the constraints on wavelength acceptance bandwidth is to engineer a configuration of the reversed domains such that momentum conservation can be simultaneously satisfied by a number of different wave lengths.[8] This approach has been realized in 1D quasiperiodically[9] or aperiodically[10] poled structures which enabled dual-[8] or multiwavelength QPM-SHG,[11] and simultaneous QPM sum frequency generation[12] in KTP and lithium tantalate ($LiTaO_3$). Since a quasiperiodic lattice can be considered as a projection from a higher-dimensional periodic structure onto a particular axis with one or more irrational coefficients,[9] one can envision an expansion of the 1D plural-QPM vector scheme into a two-dimensional (2D) periodically poled structure. The added dimension creates a number of possibilities in phase matching. For example, in the 1D periodically poled device, QPM-SHG is limited to creating an SH wave that grows solely in the direction of the fundamental beam, whereas in the 2D case the presence of $\mathbf{G}_{mn}$ vectors in the *transverse* direction can result in QPM for several propagation directions of the SH wave.[13] Theory further suggests that efficient QPM processes in the latter can lead to simultaneous phase matching of harmonic generations to a higher order.[14,15] For example, third- and fourth-harmonic generation,[16] and nonlinear SHG wavelength switching[17] are optical functionalities that can be realized from a 2D nonlinear photonic crystal (NPC).

It is well known that periodic poling of ferroelectric NPC can be facilitated by electric field action to overcome the crystal's coercive field.[18] However, one can often encounter the troublesome issue of uncontrollable domain merging due to the fringe-field effect.[19] The loss of domain fidelity can lead to a demise in the structure-related QPM vectors and is detrimental to the conversion efficiency. Although delicate poling techniques such as scanning probe[20] and direct electron beam writing[21] have been recently dem-

[a]Electronic mail: peng@cc.ee.ntu.edu.tw

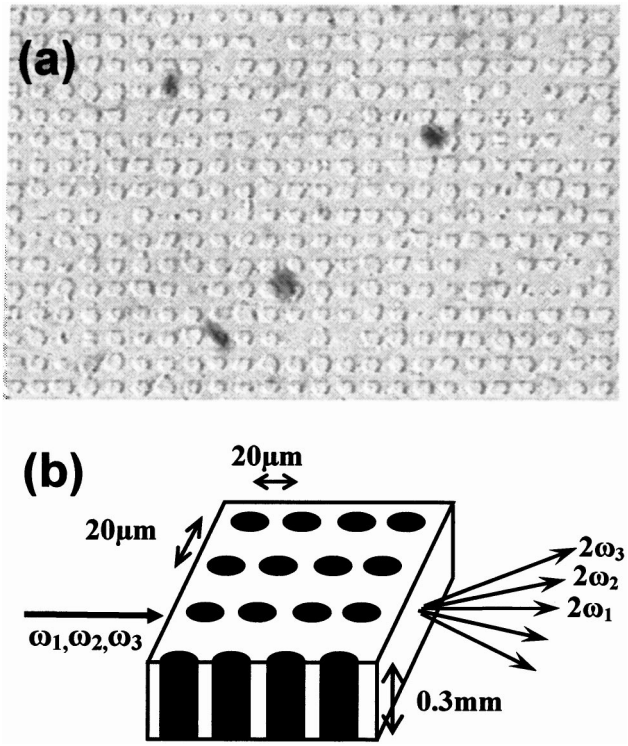

FIG. 1. (a) −Z-etched micrograph showing an NPC consisting of 2D distribution of inverted domains. The domains have a periodicity of 20×20 μm^2 on a 300-μm-thick Z-cut $LiNbO_3$ substrate. (b) Schematic drawing showing multiwavelength QPM-SHG process in (a).

onstrated to realize 2D QPM-NPC on $LiNbO_3$, for practical applications it is important to develop techniques that pole large-area QPM devices.

We have recently demonstrated a two-step poling method that can be used for fabricating large-area 2D NPC.[22] A 2D distribution of $\chi^{(2)}$ showing an orthorhombic lattice structure and domain periodicity as small as 6.6×13.6 μm^2 has been reported on a 500-μm-thick $LiNbO_3$ substrate.[23] In this letter, we report the results of our investigation on the wavelength tunability of QPM-SHG from a 2D NPC that is fabricated to quasi-phase match in the 1.55 μm communications band at room temperature (30 °C). We observed spatially distributed SHG signals whose QPM peak intensities and propagation directions depend on the pump wavelength. Furthermore, at an 8° angle of incidence relative to the crystal x axis (the $\mathbf{G}_{10}$ direction in the 2D NPC), we obtained a wavelength spread of 150 nm in phase-matched fundamental wavelengths. These phenomena are ascribed to a high-order reciprocal lattice vector ($\mathbf{G}_{mn}$) assisted QPM-SHG process in the 2D NPC.

Figure 1(a) shows the −Z-face micrograph of a 2D NPC fabricated on Z-cut $LiNbO_3$ substrate as prepared by the two-step poling technique. If one ignores the occasional imperfections in the inverted domains, one can clearly resolve a 2D distribution of inverted domains showing a periodicity of 20×20 μm^2 on a square lattice pattern. This device has an area of 6×8 mm^2. The sample edges are cut parallel to the crystalline x- and y axes and are optically polished. We note here that the spatial distribution of $\chi^{(2)}$ nonlinearity of this sample has a C_{4v} tetragonal symmetry that is different from the C_{3v} trigonal lattice symmetry of the $LiNbO_3$ host crystal. As shown below, the generation and propagation of nonlinear interacting waves in this new type of photonic crystals depend solely on the C_{4v} domain symmetry and is independent of the host's crystal symmetry. The QPM-SHG processes involving contributions from high-order reciprocal lattice vectors $\mathbf{G}_{mn}$ to satisfy the phase-matching condition for different incident wavelengths are schematically shown in Fig. 1(b). They illustrate simultaneous phase matching and spatial separation of the fundamental and harmonic waves in the 2D NPC structure.

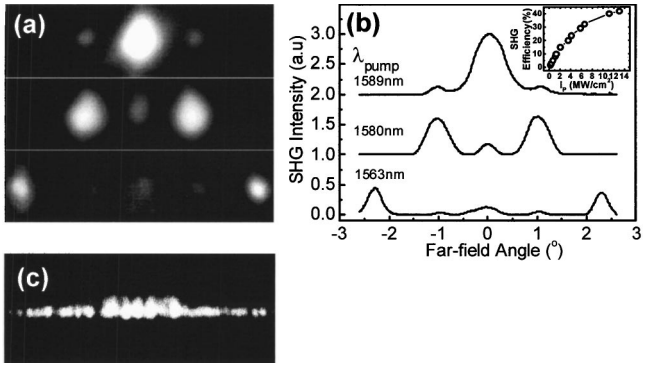

FIG. 2. (a) CCD images and (b) normalized far-field SHG intensity distribution for the sample in Fig. 1(a). The incident wavelengths are, from top to bottom, 1589, 1580, and 1563 nm. Inset: measured SHG efficiency in the $G_{1,0}$ direction for input at 1589 nm. (c) CCD image of the generated third-harmonic signal for the 1589 nm input. The pump intensity was fixed at 12.5 MW/cm^2.

The SHG measurements were conducted by using a pulsed grating-tuned periodically poled $LiNbO_3$ optical parametric oscillator operating in the 1.55-μm band.[24] By adjusting the temperature of the PPLN crystal that has a domain periodicity of 29.5 μm, output spanning a spectral range from 1450 to 1640 nm was obtained. The output peak power was 2 kW and the pulse repetition rate was 4 kHz. The fundamental pump beam was loosely focused into the polished 2D NPC sample with a beam diameter of 100 μm by a lens of 30 cm focus length, resulting in a peak intensity of 12.5 MW/cm^2 inside the crystal. A rotatable stage was attached to the sample mount to vary the azimuth angle of the sample by up to ±15°, a process equivalent to varying the incident angle of the pump beam. The SHG intensity distribution in the far field was recorded as the wavelength was changed.

Shown in Fig. 2 are the (a) CCD images and (b) normalized far-field intensity distribution of QPM-SHG signals from the sample shown in Fig. 1 for fundamental wavelengths of 1589, 1580, and 1563 nm, respectively. The SHG data were measured with the pump beam propagating along the crystal's x axis (i.e., 0° incident angle). The images were taken by placing an IR sensitive fluorescence card 10 cm away from the sample and intercepting the beams at 90°. We first note a symmetrical distribution of the QPM-SHG signals in a direction *transverse* to the propagation direction of the pump beam. Similar axial distribution of SHG signals can also be observed (not shown) as the pump beam was made to propagate along the crystal's y axis. This fourfold rotational symmetry reflects the tetragonal structure of this 2D NPC for the SHG process.[25] The peak intensity of the QPM SHG signal and its associated far-field angle were observed to be strongly dependent on the incident wavelength. We observed a 66 mW output power and a zero-degree (0°)

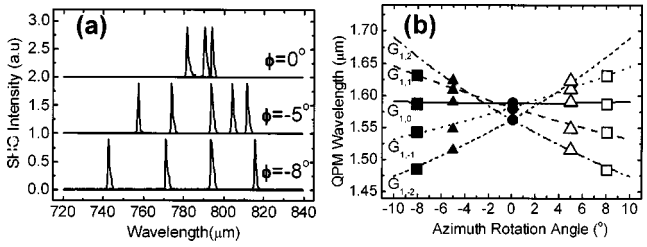

FIG. 3. (a) Normalized QPM-SHG spectra measured at sample rotation angles of 0, −5, and −8 deg and pump intensity of 12.5 MW/cm^2. (b) Dispersion curves of $G_{mn}(\phi)$ in the QPM-SHG process. Lines and dots: calculated results; symbols: experimental measurements.

far-field angle for the second harmonic of a 1589 nm fundamental pump input, while the corresponding values were (16.8 mW, ±1.13°) for a 1580 nm pump, and (6.4 mW, ±2.25°) for a 1563 nm pump, respectively. The mirror symmetry in phase-matching angle and the reduction in conversion efficiency are reminiscent of a phase-matched second-harmonic generation mechanism due to contribution from the high-order reciprocal lattice vectors $\mathbf{G}_{1,0}$, $\mathbf{G}_{1,\pm1}$, and $\mathbf{G}_{1,\pm2}$, and their corresponding second-order nonlinearities $\chi^{(2)}(\mathbf{G}_{\mathrm{mn}})$.

The inset in Fig. 2(b) shows the power dependence of the conversion efficiency for QPM-SHG due to phase matching in the $\mathbf{G}_{1,0}$ direction. The conversion efficiency is linear up to a pump intensity of ~4 MW/cm^2, and the process saturates at a pump intensity above 12 MW/cm^2. In addition to QPM-SHG, un-phase-matched higher-order harmonic generation was also observed. Figure 2(c) is an image of the third-harmonic (green) output generated by the 1589 nm pump beam at 12.5 MW/cm^2. Details of QPM third- and fourth-harmonic generation in tetragonal $\chi^{(2)}$ NPC will be presented in a forthcoming publication.

In order to grant a further understanding of QPM-SHG in tetragonal $\chi^{(2)}$ NPC, we azimuthally rotated the sample such that the internal incident angle of the input beam relative to the x (or y) axis of the 2D NPC can be varied. In doing so, the QPM-SHG process is selectively activated by a suitable reciprocal lattice vector that fulfills the phase-matching condition of $2\mathbf{k}_{\omega}+\mathbf{G}_{\mathrm{mn}}(\phi)=\mathbf{k}_{2\omega}$. Illustrated in Fig. 3(a) are the normalized SHG spectra as a function of the incident pump wavelength, limited by the tuning range of the OPO. The spectra are measured at an azimuthal rotation angle $\phi=0$, −5, and −8°, respectively, of the 2D NPC. Every peak in each spectrum corresponds to a SHG due to quasi-phase-matching for a $\mathbf{G}_{\mathrm{mn}}$ in the crystal. The spacing of phase-matchable wavelengths increases with ϕ. The span of the incident wavelengths reaches 150 nm at a −8° incidence on the crystal. Meanwhile, the spatial separation between the SHG signal also increases with ϕ.

We applied a ray-tracing method to obtain a quantitative analysis of the spatial distribution of the QPM-SHG process. This is equivalent to solving $2\mathbf{k}_{\omega}+\mathbf{G}_{\mathrm{mn}}(\phi)=\mathbf{k}_{2\omega}$, where the phase-matching wavelength λ becomes dependent on the reciprocal lattice vector $\mathbf{G}_{\mathrm{mn}}$ and the azimuthal rotation angle ϕ in the $x-y$ plane. Here, the material refractive index $n(\omega)$ is taken from Ref. 26. Illustrated in Fig. 3(b) are the derived dispersion curves overlaid with the experimental data showing the dependence of the quasi-phase-matching wavelength on $\mathbf{G}_{\mathrm{mn}}$ and ϕ. We note the inversion symmetry of the dispersion curves with respect to azimuthal rotation angle and the crossover of the $\mathbf{G}_{1,\pm\mathrm{n}}$ curves at $\phi=0°$. These are specific properties due to the C_{4v} domain symmetry of the tetragonal structure of our 2D NPC. The figure shows that at $\phi=0°$ QPM due to $\mathbf{G}_{1,\pm\mathrm{n}}$ becomes degenerate and this explains why only three peaks were observed at $\phi=0°$ as compared to five at $\phi>0$ in the experiment. Figure 3(b) also clearly illustrates an increase in quasi-phase-matchable wavelength span by a simple rotation of the 2D NPC. Hence, a bandwidth >150 nm could be obtained with an appropriately designed, possibly aperiodic inverted domain lattice distribution. This would be beneficial to applications in optical information processing.

In summary, we have demonstrated simultaneous spatial separation and wavelength tunability of QPM-SHG by using a NPC that has a 2D tetragonal distribution in $\chi^{(2)}$ and showed that it could be a promising route to increasing channel spacing and channel width in the 1.3 to 1.55 μm telecommunications band. These observations are ascribed to the unique dispersion of $\mathbf{G}_{\mathrm{mn}}(\phi)$ and nonvanishing $\chi^{(2)}(\mathbf{G}_{\mathrm{mn}})$ of the 2D NPC.

This research was supported by the National Science Council, Grant No. 92-2215-E-002-013 and –M-001-005.

[1] J. A. Armstrong, N. Bloembergen, J. Ducuing, and P. S. Pershan, Phys. Rev. **127**, 1918 (1962).
[2] Y. Yamada, N. Nada, M. Saitoh, and K. Watanabe, Appl. Phys. Lett. **62**, 435 (1993).
[3] L. E. Myers and W. R. Bosenberg, IEEE J. Quantum Electron. **33**, 1663 (1997).
[4] H. Karlsson, F. Laurell, and L. K. Cheng, Appl. Phys. Lett. **74**, 1519 (1999).
[5] M. M. Fejer, G. A. Magel, D. H. Jundt, and R. L. Byer, IEEE J. Quantum Electron. **28**, 2631 (1992).
[6] S. M. Saltiel and Y. S. Kivshar, Opt. Lett. **27**, 921 (2002).
[7] M. H. Chou, I. Brener, M. M. Fejer, E. E. Chaban, and S. B. Christman, IEEE Photonics Technol. Lett. **11**, 653 (1999).
[8] K. Fradkin-Kashi, A. Arie, P. Urenski, and G. Rosenman, Phys. Rev. Lett. **88**, 023903 (2002).
[9] S.-N. Zhu, Y.-Y. Zhu, and N.-B. Ming, Science **278**, 843 (1997).
[10] B.-Y. Gu, B.-Z. Dong, Y. Zhang, and G.-Z. Yang, Appl. Phys. Lett. **75**, 2175 (1999).
[11] H. Liu, S. N. Zhu, Y. Y. Zhu, N. B. Ming, X. C. Lin, W. J. Ling, A. Y. Yao, and Z. Y. Xu, Appl. Phys. Lett. **81**, 3326 (2002).
[12] J.-L. He, J. Liao, H. Liu, J. Du, F. Xu, H.-T. Wang, S. N. Zhu, Y. Y. Zhu, and N. B. Ming, Appl. Phys. Lett. **83**, 228 (2003).
[13] V. Berger, Phys. Rev. Lett. **81**, 4136 (1998).
[14] X.-H. Wang and B.-Y. Gu, Eur. Phys. J. B **24**, 323 (2001).
[15] A. H. Norton and C. M. De Sterke, Opt. Lett. **28**, 188 (2003).
[16] N. G. R. Broderick, R. T. Bratfalean, T. M. Monro, D. J. Richardson, and C. M. De Sterke, J. Opt. Soc. Am. B **19**, 2263 (2002).
[17] A. Chowdhury, C. Status, B. F. Boland, T. F. Kuech, and L. McCaughan, Opt. Lett. **26**, 1353 (2001).
[18] R. C. Miller and G. Weinreich, Phys. Rev. **117**, 1460 (1960).
[19] G. Rosenman, Kh. Garb, A. Skliar, M. Oron, D. Eger, and M. Katz, Appl. Phys. Lett. **73**, 865 (1998).
[20] G. Rosenman, P. Urenski, A. Agronin, Y. Rosenwaks, and M. Molotskii, Appl. Phys. Lett. **82**, 103 (2003).
[21] J. He, S. H. Tang, Y. Q. Qin, P. Dong, H. Z. Zhang, C. H. Kang, W. X. Sun, and Z. X. Shen, J. Appl. Phys. **93**, 9943 (2003).
[22] L.-H. Peng, Y.-C. Shih, S.-M. Tsan, and C.-C. Hsu, Appl. Phys. Lett. **81**, 5210 (2002).
[23] L.-H. Peng, C.-C. Hsu, and Y.-C. Shih, Appl. Phys. Lett. **83**, 3447 (2003).
[24] C.-S. Yu and A. H. Kung, J. Opt. Soc. Am. B **16**, 2233 (1999).
[25] J. F. Nye, *Physical properties of crystals* (Oxford University Press, Oxford, 1989).
[26] D. H. Jundt, Opt. Lett. **22**, 1553 (1997).